High-frequency radio wave diffraction from singly curved, convex surfaces - a heuristic approach

M.D. Casciato and K. Sarabandi

Abstract: An alternate approach is presented for the prediction of induced surface currents on perfect electric conducting (PEC) circular cylinders of large radius by observation of the asymptotic behaviour of the Fock currents. The currents are separated in the fashion of the physical theory of diffraction in terms of a uniform or physical optics component and a nonuniform or diffraction component which is highly localised to the shadow boundary. The approach can be extended to that of a general convex surface by application of known methods such as incremental-length diffraction coefficients. The case of the 2D PEC circular cylinder at normal incidence is developed first and then extended to that of oblique incidence analytically. The resulting expressions for the induced current are algebraic and are shown to be highly accurate for cylinders having radii of curvature larger than a wavelength. Total near-fields generated by this macromodelled current are in good agreement with those of the exact solution everywhere.

1 Introduction

Owing to the ever increasing demand for wireless systems, development of accurate propagation models have attained significant prominence over the past decade. Many natural terrain features exhibit both curved and doubly curved surfaces. Ridge lines in mountainous areas exhibit the features of a long curved cylinder which is essentially infinite in one dimension at high frequencies. These lines may be the result of the natural formation of the mountain chain or a feature of erosion. Geologically recent mountain chains, while exhibiting sharp-edged features, still have electrically large radii of curvature even in the HF band. This indicates that diffraction from curved surfaces, as opposed to knife-edge diffraction, is the appropriate prediction tool.

While the exact solution for a circular cylinder is known [1], the convergence properties of the resulting eigenseries deteriorate as cylinder radius increases, making it impractical for problems of large electrical size and thus alternate solutions are sought. The convergence properties of this series can be improved by applying a Watson-type integral transform [2] and the resulting expressions are the basis for many of the high-frequency techniques in use.

Current high-frequency methods for the prediction of scattering and diffraction from convex surfaces can be divided into two categories, those which are valid away from the surface (geometrical/uniform theory of diffraction (GTD/UTD), valid in regions I, II, III in Fig. 1) and those which are valid near the surface of the object (asymptotic theory of diffraction, Fock methods, valid in regions IV, V, VI in Fig. 1). None of these methods are valid in all regions around a cylinder and all suffer from significant shortcomings, as be discussed in the following Section.

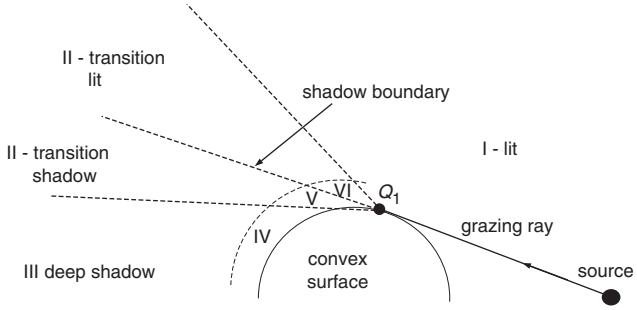

Fig. 1 *Definition of regions around a convex surface*

2 Shortcomings in existing hiqh-frequency techniques

2.1 GTD/UTD

GTD and UTD solutions are field solutions, valid away from the convex surface. GTD, developed by Keller [3] in the 1950 s is valid in the deep-lit and deep-shadow regions (I and III in Fig. 1), but not in the transition region between the shadow and illuminated areas (region II in the same Figure). In his UTD solution for plane-wave incidence, Pathak developed a method which accounts for the fields in the transition region (region II) [4]. In this approach a Watson-type transform is applied to the exact solution for a circular cylinder [2], and the resulting integrals solved by making appropriate approximations depending on the point of observation. The resulting expressions consist of a Fresnel-type integral which dominates in the transition region and a Pekeris function which dominates in the deep-lit region and should dominate in the deep-shadow region. Hussar and Albus [5] have shown that the Fresnel term in the UTD solution does not decay in the predicted fashion in the shadow region and thus the Pekeris term does not dominate as expected in this region. For source and/or

© IEE, 2004

IEE Proceedings online no. 20040089

doi:10.1049/ip-map:20040089

Paper first received 1st September and in revised form 18th November 2003. Online publishing date: 20 January 2004

The authors are with The Radiation Laboratory, Department of Electrical Engineering and Computer Science, The University of Michigan, Ann Arbor MI 48109-2122, USA

observation in the near zone of the cylinder, the UTD solution is not asymptotic (in terms of cylinder radius) and significant error is observed in field calculations as cylinder radius increases. Examples in [5] show an error of greater than 10 dB in the shadow region near transition (the boundary between regions II and III in Fig. 1) which increases to near 40 dB in the deep-shadow region. In [5], the Pathak formulation is adjusted with a correction consisting of an infinite series which produces very accurate results. The method is not valid however, for both source and observation very near the surface and the number of terms necessary for convergence of the series is directly proportional to the distance of both source and observation from the cylinder surface and increases as either one or both are moved away from the cylinder.

2.2 Asymptotic theory of diffraction: evaluation of Fock-type integrals

For observation points on or near the cylinder surface, asymptotic field solutions based on Fock theory [6] are usually applied. These solutions in general consist of solving the canonical Fock-type integrals, which are functions of a universal variable, in either a numerical fashion or by referencing tabulated data. In the deep-lit and deep-shadow regions these integrals reduce to an asymptotic and residue series, respectively. These integrals are highly oscillatory in nature and difficult to evaluate numerically. The universal variable is a function of the observation distance from the shadow boundary along the circumference of the cylinder. As observation moves into the lit region from the shadow boundary, the convergence properties of the Fock integrals degrade and eventually will fail to converge. As this is a function of distance from the shadow boundary, the point where the integrals will no longer converge is more localised to the shadow boundary as the cylinder radius increases. At this point in the lit region a transition must be made to the asymptotic series. For cylinders of large radii, this transition occurs at a point in the lit region where the asymptotic series does not converge well and a significant discontinuity in the surface current occurs. A method has been developed by Pearson [7] which improves the convergence properties of these types of integrals, but does not effect the region of convergence on the cylinder surface. Logan, in his extensive work on diffraction theory, has published tabulated data on the Fock integrals [8] for observation at and around the shadow boundary. The extent of the tabulated data into the lit region, however, is limited by the region of convergence of the Fock integrals.

As an example of the convergence problems of the Fock-type integrals in the lit region, Fig. 2 shows the TM (incident electric field parallel to the cylinder axis) and TE (incident magnetic field parallel to the cylinder axis) current distributions, for cylinders of radius 10, 15 and 20λ, generated by the Fock solution. Note that on these plots 0.25 corresponds to normal incidence, in the deep-lit region, with −0.25 and 0.75 both corresponding to the deep-shadow region. What is apparent in these curves is the convergence problems of the Fock-type integrals in the deep-lit region, and the increasing region of nonconvergence as cylinder radius increases. While Fock functions and Fock integrals are described in more detail in Section 3.1 the reason for the convergence problems stems from evaluation of the Airy function and its derivative contained within the integrand of the Fock functions. As observation is moved more deeply into the lit region from the shadow boundary, the Fock integrand becomes more oscillatory, and evaluation of these Airy functions more difficult. The point in the lit region where the Fock integrals can no longer be

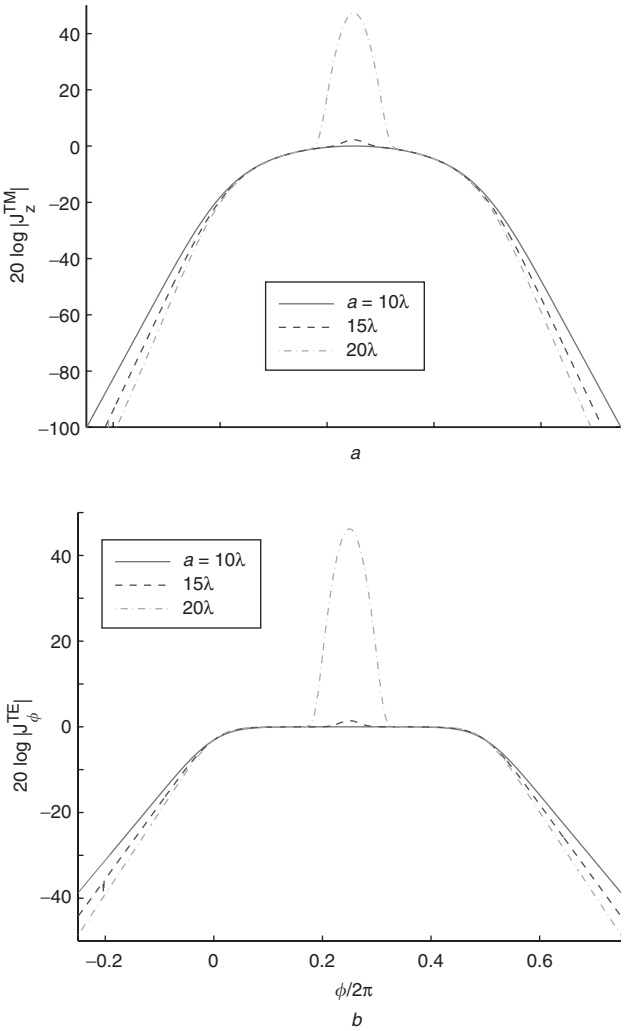

Fig. 2 *Total current magnitude (dB) of Fock currents around the full circumference of PEC cylinder excited at normal incidence angle $\theta^i = \pi/2$. $(\phi/2\pi) = 0$ is equivalent to a point on top of the cylinder at the shadow boundary, with $(\phi/2\pi) = -0.25$ in the deep-shadow region*
a $|J_z^{TM}|$
b $|J_\phi^{TE}|$

evaluated is not deep enough into the lit region for the asymptotic approximation to the Fock integrals to be of practical accuracy. The effect of the nonconvergence of the Fock-type integrals on the total electric fields can be seen in Fig. 3. In this Figure a comparison is shown of the total TM fields generated by the macromodelled currents, developed later in this paper, to those generated by the Fock current functions, for a cylinder of radius 15λ. Observation is 1λ off the surface of the cylinder. Note in these plots that −90 and +90 correspond to the deep-shadow and deep-lit regions, respectively. Referring to the Fock currents in Fig. 2, for a cylinder of radius 15λ, it is apparent that the solution did not converge at near normal incidence, in the deep-lit region. This discrepancy is apparent in the accuracy of the total fields generated by these currents, as observed in Fig. 3 in both the deep-lit and deep-shadow regions. It can be shown by asymptotic evaluation of the radiation integrals that in the deep-lit and deep-shadow regions the main contributor to the scattered fields is the current in the deen-lit region, around normal incidence, the same area where the convergence problems arise in generating the Fock currents. This is evident in the total fields in Fig. 3 as the most significant error observed in

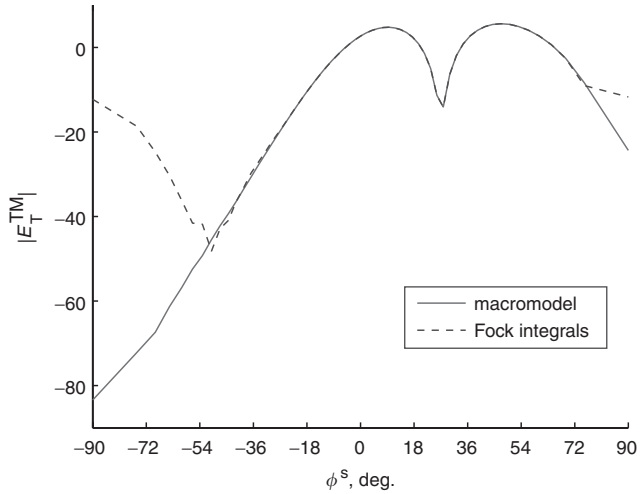

Fig. 3 *Magnitude (dB) of total TM E-fields 1λ off the surface of a 15λ PEC cylinder excited by a plane wave at normal incidence $\theta^i = \pi/2$, with -90° corresponding to deep shadow and 90° corresponding to normal incidence (deep lit)*

the fields generated by the Fock solution are in these regions.

Owing to the discussed shortcomings with current high-frequency techniques, it is desired to develop a method for predicting the fields scattered by a circular cylinder that is highly accurate and valid in all regions around the cylinder. If the induced surface currents could be calculated simply, quickly, and in an accurate fashion, fields in all regions around the cylinder could be calculated by application of the radiation integrals. With this as a motivation, a heuristic method is developed, which predicts the behaviour of the induced surface currents on a perfect electric conducting (PEC) circular cylinder, when excited by a plane wave at oblique incidence angles. The induced surface currents are decomposed in the manner of the physical theory of diffraction (PTD) [9] in terms of a uniform or physical optics (PO) component and a nonuniform or diffraction component. In using this decomposition the proposed method can be described as a form of PTD for convex surfaces. To predict these diffraction currents, a set of macromodels are developed using a combination of the asymptotic behaviour of the Fock currents [2, 4, 6] and the exact solution for oblique incidence. These macromodels are used to predict the high-frequency behaviour of the diffraction current as a function of k_0a, where k_0 is the free-space propagation constant and a the cylinder radius, to a very high degree of accuracy. To predict the induced diffraction currents, these macromodels are simply applied to a set of reference data generated by the exact solution for a cylinder of moderate radius. These macromodels are valid for cylinders of radius $a > \lambda$ and the resulting total surface currents are highly accurate. The observed error in magnitude $e_\parallel$ is less than -60 dB, where $e_\parallel = 20\log(\|\boldsymbol{J}_{ex}| - |\boldsymbol{J}_{mm}\|)$ and $\boldsymbol{J}_{ex}$ and $\boldsymbol{J}_{mm}$ are the exact and macromodelled total induced surface currents, respectively. The error in phase $e_\angle = \angle\boldsymbol{J}_{ex} - \angle\boldsymbol{J}_{mm}$ is less than 0.1° everywhere except in the deep-shadow region.

3 Development of macromodel

Consider an infinite right-circular PEC cylinder, illuminated by a monochromatic plane wave, as shown in Fig. 4. The cylinder is oriented along the z-axis with θ_i, defined from the z-axis and confined to the y–z plane and ϕ defined from the x-axis and positive towards the y-axis.

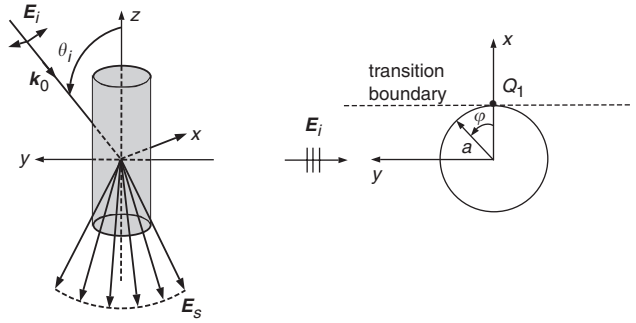

Fig. 4 *Scattering geometry of an infinite cylinder*

The propagation constant of the plane wave $\boldsymbol{k}$ is defined as $\boldsymbol{k} = -k_0\cos\theta_i\,\hat{z} - k_0\sin\theta_i\,\hat{y}$. For the problem of an infinite cylinder the z-component of the propagation constant of the scattered field must match that of the incidence field, requiring that scattered fields be confined to the specular cone, as shown in Fig. 4.

Decomposing the induced surface current in the manner of PTD we write the diffraction current $\boldsymbol{J}_D$ as $\boldsymbol{J}_D = \boldsymbol{J}_{ex} - \boldsymbol{J}_{PO}$ where $\boldsymbol{J}_{PO}$ is the PO current given by

$$\boldsymbol{J}_{PO} = \begin{cases} 2\hat{\boldsymbol{n}} \times \boldsymbol{H}_i & \text{lluminated region} \\ 0; & \text{shadow region} \end{cases} \tag{1}$$

Depending on the polarisation of the incident field, on the cylinder surface

$$\boldsymbol{H}_i = \begin{cases} -H_0\hat{x}; \\ \text{TM case (transverse magnetic to } z\text{−axis)}, \\ H_0(\sin\theta_i\hat{z} - \cos\theta_i\hat{y}); \\ \text{TE case (transverse electric to } z\text{−axis)}. \end{cases} \tag{2}$$

The objective is to macromodel $\boldsymbol{J}_D(\phi) = |\boldsymbol{J}_D(\phi)|e^{j\psi}$ with algebraic expressions, which are in terms of k_0a, and for the general case of oblique incidence and arbitrary polarisation. This is accomplished by simply applying appropriate scaling (expansion or contraction of co-ordinate ϕ) and weighting (multiplicative factor) functions to a reference data consisting of the magnitude and phase components of the exact diffraction current for a specific radius cylinder. In practice, to apply the macromodel, reference data is generated for a cylinder of moderate k_0a using the exact solution for normal incidence (2-D case). The macromodel is then applied to this reference data to generate extremely accurate surface currents for an infinite PEC cylinder of any radius larger than 1λ and for the general case of oblique incidence.

In the remainder of this Section the Fock formulations for the generation of induced surface currents on a PEC cylinder are reviewed along with observations relevant to developing the macromodel. The macromodel will then be developed for the 2-D case (TM z and TE ϕ currents only are excited) in both the shadow and lit regions. The macromodel for the 2-D currents is then extended to the case of oblique incidence in a simple fashion. All macromodelled currents, including the additional z-directed current excited at oblique incidence for the TE case, are generated from the reference data for a cylinder excited at normal incidence (2-D case). In all cases the macromodel is also applied to generate the induced surface currents on a half-cylinder ($-\pi/2 \le \phi \le \pi/2$ in Fig. 4) and this current simply mirrored to generate currents around the full circumference of the cylinder.

3.1 Fock theory

The macromodel of the diffraction current $\boldsymbol{J}_D$ predicts the behaviour of this current as a function of k_0a by observing the asymptotic behaviour in the analytical expressions for the Fock currents. These currents indicate the general behaviour of the diffraction current as a function of k_0a for all regions on the cylinder surface. The analytical expressions for currents on the surface of a PEC cylinder are given by Pathak [4]. These expressions are a special case of the Fock currents in which the canonical Fock integrals are approximated by a Taylor-series expansion in the close neighbourhood of the surface and reduce to the Fock solution on the cylinder surface. In the shadow region the Fock currents for TM and TE cases are given by

$$\boldsymbol{J}_s^{TM} = \frac{U_i(Q_1)}{jk_0Z_0} e^{jk_0a\phi} \left(\frac{k_0}{m}\right) \tilde{g}(Z)\hat{z} \tag{3}$$

$$\boldsymbol{J}_s^{TE} = -U_i(Q_1) e^{jk_0a\phi} g(Z)\hat{\phi} \tag{4}$$

where the subscript s denotes the shadow region. In (3) and (4) $U_i(Q_1)$ is the incident electric field for the TM case and the incident magnetic field for the TE case evaluated on the cylinder surface at the shadow boundary (point Q_1) shown in Fig. 1. Also in (3) and (4), $m = (k_0a/2)^{1/3}$, Z_0 is the characteristic impedance of free space and $\tilde{g}(Z)$ and $g(Z)$ are the Fock functions given by

$$\tilde{g}(Z) = \frac{1}{\sqrt{\pi}} \int_{-\infty}^{+\infty} d\tau \frac{e^{-jZ\tau}}{w_2(\tau)} \tag{5}$$

$$g(Z) = \frac{1}{\sqrt{\pi}} \int_{-\infty}^{+\infty} d\tau \frac{e^{-jZ\tau}}{w_2'(\tau)} \tag{6}$$

where $Z = -m\phi$ and is defined in the shadow region only, and w_2 is the Airy function as defined in [4]. In the lit region the Fock currents are given by

$$\boldsymbol{J}_l^{TM} = \frac{U_i(P)}{jk_0Z_0} e^{-j\frac{(Z')^3}{3}} \left(\frac{k_0}{m}\right) \tilde{g}(Z')\hat{z} \tag{7}$$

$$\boldsymbol{J}_l^{TE} = -U_i(P) e^{-j\frac{(Z')^3}{3}} g(Z')\hat{\phi} \tag{8}$$

where the subscript l denotes the lit region and the incident field U_i is evaluated at the point P on the surface of the cylinder, in the lit region, where the value of the induced surface current is desired. In (7) and (8), $\tilde{g}$ and g are functions of Z', where $Z' = -m\sin\phi$ and is defined in the lit region only. To construct the macromodel for the induced surface diffraction currents the following observations of the asymptotic behaviour of the Fock currents are noted:

(i) The factor m, implicit in both Z (shadow region) and Z' (lit region), is proportional to $(k_0a)^{1/3}$.

(ii) In the shadow region the Fock functions for both the TM and TE cases can be evaluated in terms of a residue series which is a function of Z. This indicates that the macromodel developed for the complex diffraction current in the shadow region is valid throughout the shadow region.

(iii) The TM current, given by (3) in the shadow region and (7) in the lit region, has a weighting factor of k_0/m.

(iv) In the deep-lit region $\tilde{g}(Z')$ and $g(Z')$ can be expanded into an asymptotic series given by

$$\tilde{g}(Z') = -2jZ'e^{j\frac{(Z')^3}{3}} \left\{1 + \frac{j}{4Z'^3} + \frac{1}{2Z'^6}\cdots\right\} \tag{9}$$

$$g(Z') = 2e^{j\frac{(Z')^3}{3}} \left\{1 - \frac{j}{4Z'^3} - \frac{1}{Z'^6}\cdots\right\} \tag{10}$$

(v) The phase component of the Fock currents can be decomposed into a highly oscillatory and slowly varying or gentle phase component. If we designate the exponential of the diffraction current by

$$e^{j\psi_h(k_0a,\phi)+j\psi_g(k_0a,\phi)} \tag{11}$$

where the subscripts h and g indicate the highly oscillatory and gentle phase components of the current, respectively, the highly oscillatory phase terms are known in all regions.

In the lit region, $\psi_h(k_0a,\phi)$ is simply the phase of the incident field or

$$\psi_h(k_0a,\phi) = k_0a\sin\phi \tag{12}$$

and in the shadow, $\psi_h(k_0a,\phi)$ is a linear-phase term given by

$$\psi_h(k_0a,\phi) = k_0a\phi \tag{13}$$

The remaining gentle phase component $\psi_g(k_0a,\phi)$ is monotonic in both the lit and shadow regions and this is the component of the phase which will be macromodelled.

3.2 2-D case, normal incidence

To generate diffraction currents for cylinders of arbitrary radius the macromodels are applied to reference data consisting of the diffraction currents from a cylinder of moderate radius, generated from the exact solution. The macromodels described in this Section are developed using reference data for the TM case from a cylinder of radius 20λ and for the TE case a cylinder of radius 50λ. Reasons for the choice of these cylinder sizes to generate the reference currents are given in more detail in Section 4.

3.2.1 Magnitude, shadow region: To begin development of the macromodel for the diffraction current magnitude in the shadow region, we again note that the Fock currents in the shadow region can be evaluated in terms of a residue series, and thus the macromodel developed is valid throughout the shadow region. Recall that the factor m is proportional to $(k_0a)^{1/3}$ and is implicit in the argument Z of both the $\tilde{g}(Z)$ and $g(Z)$ terms in (3) and (4). This implies a scaling of co-ordinate ϕ by $(k_0a)^{1/3}$ for both the TM and TE cases. For the TM case, a factor of $(1/m)$ is observed in (3) implying a multiplicative or weighting factor for the TM current of $(k_0a)^{-(1/3)}$. Observation of (4) shows no weighting of the TE currents in the shadow region. Examination of diffraction currents generated by the exact solution, however, shows that the TM weighting factor is approximate and that there is a small weighting of the TE currents. Empirical expressions are determined, which are functions of k_0a, to adjust for this. Applying these scaling and weighting factors we now define the macromodel in the shadow region, relating the diffraction current magnitudes on a cylinder of arbitrary radius a_2 to that of the reference cylinder of radius a_1 by

$$|\boldsymbol{J}_D^{TM,TE}(k_0a_2,\,\phi)| = \alpha_s^{TM,TE} \left|\boldsymbol{J}_D^{TM,TE}\left(k_0a_1,\,\left(\frac{k_0a_1}{k_0a_2}\right)^{(1/3)}\phi\right)\right| \tag{14}$$

The weighting factor $\alpha_s^{TM,TE}$ is given by

$$\alpha_s^{TM,TE} = \left(\frac{k_0a_1}{k_0a_2}\right)^{W_s^{TM,TE}(k_0a_2)} \tag{15}$$

where $W_s^{TM,TE}(k_0a_2)$ is a function of k_0a and is asymptotic in k_0a, with limiting values of approximately (1/3) for the TM case and 0 for the TE case for cylinders of large k_0a. Recognising the asymptotic behaviour of $W_s^{TM,TE}(k_0a_2)$, expressions for it are obtained by fitting an exponential to the curves generated by the exact solution, and are given by

$$W_s^{TM}(k_0a_2) = \begin{cases} 0.3373 + 0.009562e^{-0.1176k_0a_2} \\ \quad +0.0045531e^{-0.04896k_0a_2} \quad \text{for } 1\lambda < a_2 < 20\lambda \\ 0.3348 + 0.005651e^{-0.01103k_0a_2} \\ \quad +0.001721e^{-0.0024k_0a_2} \quad \text{for } 15\lambda < a_2 < +\infty \end{cases} \tag{16}$$

$$W_s^{TE}(k_0a_2) = \begin{cases} -0.02086 + 0.01708(1 - e^{-0.09979k_0a_2}) \\ \quad +0.006827(1 - e^{-0.002576k_0a_2}) \quad \text{for } 1\lambda < a_2 < 50\lambda \\ -|0.005987 - 0.007045(1 - e^{-0.006046k_0a_2})| \\ \quad \text{for } 20\lambda < a_2 < +\infty \end{cases} \tag{17}$$

3.2.2 Magnitude, lit region: To macromodel the magnitude of the J_{Dz}^{TM} and $J_{D\phi}^{TE}$ diffraction current in the lit region, note that the behaviour of the diffraction current as a function of (k_0a) transitions from the shadow boundary to the deep-lit region, and thus expressions which are also a function of ϕ, must be developed. Sigmoidal functions are then used to model the transition from the shadow boundary to the deep-lit region as a function of ϕ.

For the TM case, we note that in the transition from shadow to lit regions the magnitude of the diffraction current is continuous across the shadow boundary; therefore (14) and (15) apply in the lit region at and very near the shadow boundary. However, for the TE case, the magnitude of the diffraction current across the transition from shadow to lit is discontinuous. The PO current for the TE case undergoes an abrupt transition from a constant in the lit region to zero at the shadow boundary. The exact TE current changes gradually and monotonically across the shadow boundary. Remembering that the diffraction current is defined as $\boldsymbol{J}_D = \boldsymbol{J}_{ex} - \boldsymbol{J}_{PO}$, the abrupt change in the PO current causes a phase reversal in the TE diffraction current and an abrupt change in the magnitude of the TE diffraction current across the shadow boundary. This can be seen in Fig. 5*b*. It was determined empirically by observation of the exact solution that, near the shadow boundary in the lit region, (14) and (15) can be applied for the TE case if the factor $W_s^{TE}(k_0a_2)$ is modified as follows:

$$W_{l,sb}^{TE}(k_0a_2) = -2.25W_s^{TE}(k_0a_2) \tag{18}$$

where the subscript *l*, *sb* implies the lit region at the shadow boundary.

To define the magnitude of the diffraction currents in the deep-lit region recall that, in the deep-lit region, the surface currents are described by the asymptotic expansions of the Fock functions, $\tilde{g}(Z')$ and $g(Z')$ given in (9) and (10). The first terms in (9) and (10) are the PO currents, with higher-order terms defining the nonuniform or diffraction currents. In the deep-lit region, only the second terms in (9) and (10) are needed to evaluate the diffraction current. Substituting the second term in (9) and (10) for $\tilde{g}(Z')$ and $g(Z')$ in (7) and (8) and evaluating the resulting expression indicates that the diffraction current in the deep-lit region is weighted by a coefficient of $1/(k_0a)$, implicit in the $(Z')^3$ term in the denominator of the second term in (9) and (10) (recall that $m = (k_0a/2)^{1/3}$). There is no scaling of the argument ϕ in the deep-lit region for either the TM or TE case.

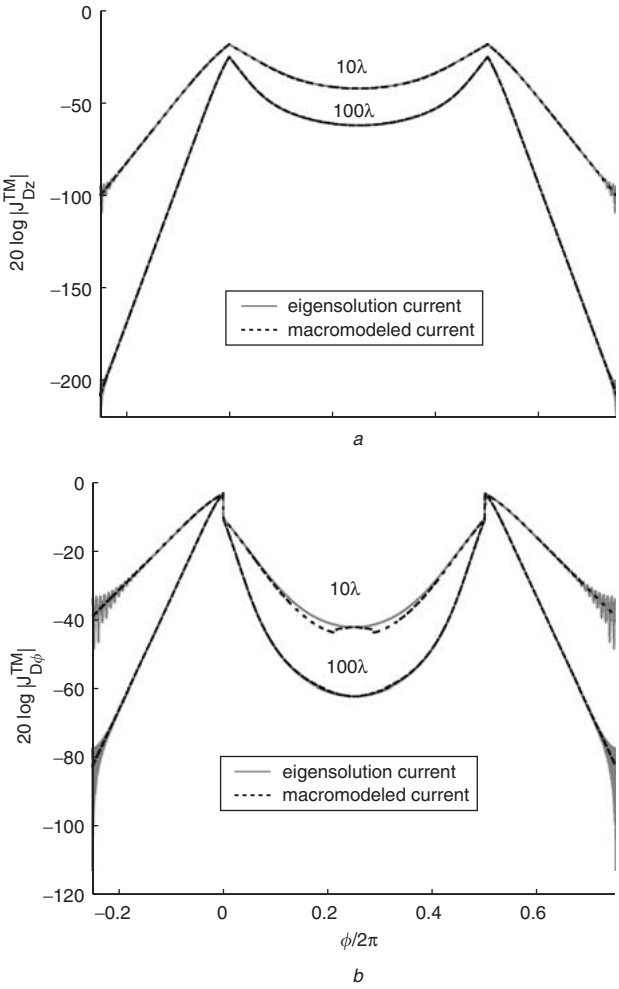

Fig. 5 *Diffraction current magnitude (dB) around full circumference of 10 and 100λ PEC cylinders excited at normal incidence angle, $\theta_i = \pi/2$, $(\phi/2\pi) = 0$ is equivalent to point on top of cylinder. δ at the shadow boundary, with $(\phi/2\pi) = -0.25$ in the deep-shadow region*
a $|J_{Dz}^{TM}|$
b $|J_{D\phi}^{TE}|$

Having established the behaviour of the diffraction current magnitudes at the shadow boundary and in the very deep-lit region, a function must be specified to change from the shadow boundary to the deep-lit region and as a function of ϕ. Defining the relationship between the diffraction current, magnitude in the lit region on a cylinder of arbitrary radius a_2 and the reference cylinder of radius a_1 as

$$|\boldsymbol{J}_D^{TM,TE}(k_0a_2, \phi)| = \alpha_l^{TM,TE} \left| \boldsymbol{J}_D^{TM,TE}\left(k_0a_1, \left(\frac{k_0a_1}{k_0a_2}\right)^{S_l^{TM,TE}(\phi)} \phi\right)\right| \tag{19}$$

where $\alpha_l^{TM,TE}$ is the weighting factor in the lit region given by

$$\alpha_l^{TM,TE}(k_0a_2, \phi) = \left(\frac{k_0a_1}{k_0a_2}\right)^{W_l^{TM,TE}(\phi)} \tag{20}$$

and the functions $S_l^{TM,TE}(\phi)$ and $W_l^{TM,TE}(\phi)$ in (19) and (20) are the powers of the scaling and weighting expressions for the TM and TE cases, and define the transition in the lit region from shadow boundary to deep lit as a function of ϕ. Recognising that these functions ought to be very gentle, with known values at the shadow boundary ($\phi = 0$) and deep-lit region ($\phi = \pi/2$), sigmoidal functions are chosen to describe the transition. S_l and W_l are given by the following expressions:

$$S_l(\phi) = b - \frac{c}{1 + e^{-d(\frac{\phi}{2\pi} - \phi_0)}} \tag{21}$$

and

$$W_l(\phi) = b + \frac{c}{1 + e^{-d(\frac{\phi}{2\pi} - \phi_0)}} \tag{22}$$

where b, c, d, and ϕ_0 in (21) and (22) are constant parameters determined by optimisation. To calculate the optimal values for these coefficients, a simple search algorithm is employed. The algorithm searches through a range of values for d and ϕ_0 (b and c are defined in terms of d and ϕ_0) and determines the values which produce minimum error between diffraction current generated by the exact solution and diffraction current generated by the macromodel. The optimal values of b, c, d, and ϕ_0 for a test cylinder of radius $a = 200\lambda$ (as the transitional behaviour of the diffraction currents through the lit region is a function of ϕ only, any cylinder of radius larger than the reference cylinders can be used as a test cylinder for optimisation of these parameters) are given in Table 1 with the exception of the b and c coefficients for the weighting functions $W_l^{TM,TE}$. Remembering that the weighting functions $W_l^{TM,TE}$ at the shadow boundary are also functions of k_0a, then the coefficients b and c for the weighting functions in the lit region must also be functions of k_0a as well as ϕ. Defining these coefficients as $b_w^{TM}, b_w^{TE}, c_w^{TM}$ and c_w^{TE} in Table 1, they can be calculated in terms of the TM and TE weighting functions in the lit region and at the shadow boundary. At the shadow boundary, W_l^{TM} is defined by W_s^{TM} (is given by (16)) and W_l^{TE} is defined by $W_{l,sb}^{TE}$ (W_l^{TE} defined at the shadow boundary given in (18)). These coefficients as functions of k_0a are given by

$$c_w^{TM} = (1 - W_s^{TM})\left[\frac{1}{1 + e^{-d(1-\phi_0)}} - \frac{1}{1 + e^{d\phi_0}}\right]^{-1} \tag{23}$$

$$c_w^{TE} = (1 - W_{l,sb}^{TE})\left[\frac{1}{1 + e^{-d(1-\phi_0)}} - \frac{1}{1 + e^{d\phi_0}}\right]^{-1} \tag{24}$$

$$b_w^{TM,TE} = 1 - c_w^{TM,TE}\left[\frac{1}{1 + e^{-d(1-\phi_0)}}\right] \tag{25}$$

Table 1: Optimised parameters for sigmoidal transition functions

	d	ϕ_0	b	c
$S_l^{TM}(\phi)$	9.903	0.5650	0.3346	0.3391
$S_l^{TE}(\phi)$	10.6	0.6630	0.3336	0.3430
$W_l^{TM}(k_0a, \phi)$	10.025	0.5268	b_w^{TM}	c_w^{TM}
$W_l^{TE}(k_0a, \phi)$	8.5	0.610	b_w^{TE}	c_w^{TE}

3.2.3 Phase, all regions: Having developed an accurate model for the magnitude of the complex diffraction current, the next step is to macromodel the gentle phase component for the 2-D case, described in (11). This gentle phase component, $\psi_g(k_0a, \phi)$, is monotonic for the TM case and piecewise monotonic for the TE case, as shown in Figs. 6*a* and 6*b* respectively. The observed behaviour of the Fock currents again allows for prediction of the asymptotic behaviour of this gentle phase factor in an accurate fashion. In the shadow region, as already noted, a residue series is applied to calculate the complex surface currents. Recall that this residue series is a function of Z which again implies a scaling of the argument ϕ, implicit in Z, by $(k_0a)^{(1/3)}$ for both the TM and TE cases. This scaling was determined to be valid for the gentle phase function in the shadow region. In addition, it was also determined empirically that this scaling is an acceptable approximation in the lit region. While no weighting of the gentle phase component is implied by observation of the Fock currents, it was observed that a small offset of $\psi_g(k_0a, \phi)$ as a function of k_0a is necessary, and this offset is determined by observing the exact solution. Thus the expression relating the gentle

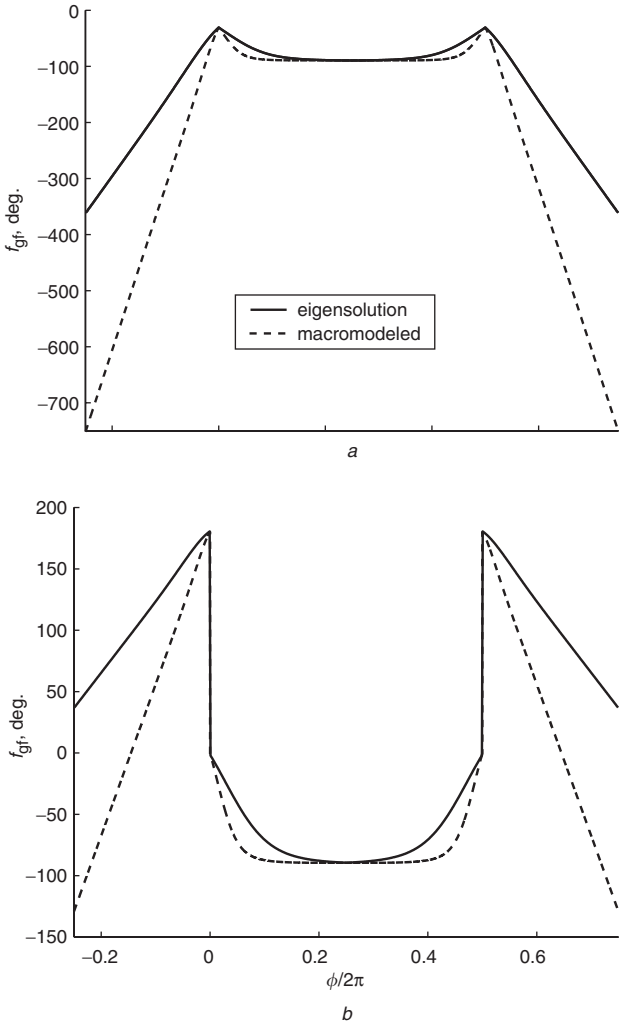

Fig. 6 *Gentle phase component (degrees) around full circumference of 10 and 100λ PEC cylinders excited at normal incidence angle, $\theta_i = \pi/2$, $(\phi/2\pi) = 0$ is equivalent to a point on top of the cylinder at the shadow boundary, with $(\phi/2\pi) = -0.25$ in the deep-shadow region*
a f_g^{TM}
b f_g^{TE}

phase component for a cylinder of radius a_2 to the reference cylinder of radius a_1 is

$$\psi_g^{TM,TE}(ka_2,\ \phi) = O^{TM,TE} + \psi_g^{TM,TE}\left(ka_1,\ \left(\frac{k_0a_1}{k_0a_2}\right)^{(1/3)}\phi\right) \tag{26}$$

where $O^{TM,TE}$ is the adjustment factor for the gentle phase term and is given, for the TM case in all regions and the TE case in the shadow region, by

$$O_{l,s}^{TM,TE}(k_0a_2) = \begin{cases} -0.07255 + 0.05857(1 - e^{-0.08778k_0a_2}) \\ \quad +0.01777(1 - e^{-0.01231k_0a_2}) \quad \text{for } 1\lambda < a_2 < 20\lambda \\ -0.01608 + 0.01701(1 - e^{-0.01592k_0a_2}) \\ \quad +0.005747(1 - e^{-0.002158k_0a_2}) \quad \text{for } 15\lambda < a_2 < +\infty \end{cases} \tag{27}$$

As mentioned earlier the PO current for the TE case undergoes an abrupt transition at the shadow boundary causing a phase reversal in the diffraction current. Thus ψ_g^{TE} is discontinuous across the shadow boundary as seen in Fig. 6*b*. Consequently O^{TE} is also discontinuous across the shadow boundary. The relationship between O^{TE} in the shadow and lit regions was determined empirically to be

$$O_l^{TE}(k_0a_2) = -2O_s^{TE}(k_0a_2) \tag{28}$$

3.3 Oblique incidence

To extend the macromodel to the case of oblique incidence for both polarisations, a comparison is made between the exact solution for a PEC circular cylinder, when excited at both normal and oblique incidences [1]. It is observed that the oblique solution can be obtained from that of normal incidence by making the following modifications:

- $k_0a \rightarrow k_0a\sin\theta_i$, incident wave simply 'sees' an effectively smaller cylinder
- a multiplicative, progressive phase factory $e^{jk_0\cos\theta_i z}$ is added
- TE current is modified by sin θ_i (projection factor).

An additional z-directed current is generated for the TE case at oblique incidence angles. This current is not independent, and its dependence on $J_\phi^{TE}(k_0a,\ \phi,\ \theta_i)$ is given by [1]

$$J_z^{TE}(k_0a,\ \phi,\ \theta_i) = \frac{j\cot\theta_i}{k_0a\sin\theta_i}\frac{\partial}{\partial\phi}J_\phi^{TE}(k_0a,\ \phi,\ \theta_i) \tag{29}$$

Having an expression for $J_\phi^{TE}(k_0a,\ \phi,\ \theta_i)$ the expression for $J_z^{TE}(k_0a,\ \phi,\ \theta_i)$ can be obtained. However, remembering that $J_\phi^{TE}(k_0a,\ \phi,\ \theta_i)$ is composed of a PO component $J_{PO\phi}^{TE}(k_0a,\ \phi,\ \theta_i)$ and a diffraction component $J_{D\phi}^{TE}(k_0a,\ \phi,\ \theta_i)$, the magnitude and phase of $J_{D\phi}^{TE}(k_0a,\ \phi,\ \theta_i)$ is macromodelled separately and evaluation of

$$\frac{\partial}{\partial\phi}J_{D\phi}^{TE}(k_0a,\ \phi,\ \theta_i)$$

is not straightforward. A procedure is outlined for the calculation of

$$\frac{\partial}{\partial\phi}J_{D\phi}^{TE}(k_0a,\ \phi,\ \theta_i)$$

As mentioned, to generate $J_z^{TE}(k_0a,\ \phi,\ \theta_i)$ the term

$$\frac{\partial}{\partial\phi}J_{D\phi}^{TE}(k_0a,\ \phi,\ \theta_i)$$

must be evaluated in terms of the macromodel. The expression for $J_{D\phi}^{TE}(k_0a,\ \phi,\ \theta_i)$ in terms of the macromodel is of the form given by (14), (19) and (26) or

$$J_{D\phi}^{TE}(k_0a_2,\ \phi) = \alpha^{TE}\left|J_{D\phi}^{TE}\left(k_0a_1,\ \left(\frac{k_0a_1}{k_0a_2}\right)^{S^{TE}(k_0a_2,\phi)}\phi\right)\right| \times e^{\{jO^{TE}(k_0a_2)+j\psi_g^{TE}(k_0a_1,(\frac{k_0a_1}{k_0a_2})^{(1/3)}\phi)\}}e^{j\psi_h(k_0a_2,\phi)} \tag{30}$$

The derivative of (30) with respect to ϕ is straightforward with the exception of two terms. These terms are the derivatives of the magnitude and gentle phase component of the reference cylinder, and their evaluation in terms of the macromodel is not obvious. These terms are given by

$$\frac{\partial}{\partial\phi}\left|J_{D\phi}^{TE}\left(k_0a_1,\ \left(\frac{k_0a_1}{k_0a_2}\right)^{s^{TE}(k_0a_2,\phi)}\phi\right)\right| = \frac{\partial}{\partial\tilde{\phi}}|J_{D\phi}^{TE}(k_0a_1,\ \tilde{\phi})|\frac{\partial\tilde{\phi}}{\partial\phi} \tag{31}$$

where

$$\tilde{\phi} = \left(\frac{k_0a_1}{k_0a_2}\right)^{S^{TE}(k_0a_2\phi)}\phi \tag{32}$$

and

$$\frac{\partial}{\partial\phi}\psi_g^{TE}\left(k_0a_1,\ \left(\frac{k_0a_1}{k_0a_2}\right)^{(1/3)}\phi\right) = \left(\frac{k_0a_1}{k_0a_2}\right)^{(1/3)}\frac{\partial}{\partial\tilde{\phi}}\psi_g^{TE}(k_0a_1,\ \tilde{\phi}) \tag{33}$$

where S^{TE} in (31) is the scaling factor for the TE case, given by 1/3 in the shadow region and the sigmoidal transition function S_l^{TE} in the lit region, as described previously. While evaluation of $\partial\tilde{\phi}/\partial\phi$ in (31) is simple, evaluation of the other derivatives to the right of the equal sign in (31) and (33) is not. To evaluate these terms, we note that

$$\frac{\partial}{\partial\tilde{\phi}}|J_{D\phi}^{TE}(k_0a_1,\tilde{\phi})|$$

and

$$\frac{\partial}{\partial\tilde{\phi}}\psi_g^{TE}(k_0a_1,\tilde{\phi})$$

in (31) and (33) are derivatives of the entire argument and are therefore independent of k_0a. We can therefore calculate these terms directly from diffraction current in the reference data. To do this we simply define the diffraction current in terms of its real and imaginary parts or $J_{D\phi}^{TE} = X + jY$. The derivative of the magnitude is then given by

$$\frac{\partial}{\partial\tilde{\phi}}|J_{D\phi}^{TE}| = \frac{XX' + YY'}{\sqrt{X^2 + Y^2}} \tag{34}$$

and the derivative of the phase by

$$\frac{\partial}{\partial\tilde{\phi}}\psi_g^{TE} = \frac{Y'X - YX'}{X^2 + Y^2} \tag{35}$$

4 Validation and simulations

In the previous Section, a macromodel was developed which relates the diffraction current on a PEC cylinder of arbitrary radius a_2 to that of a reference cylinder of radius a_1, for plane-wave excitation at oblique angles. In practice, this macromodel allows the complex diffraction currents for any cylinder with radius a_2 illuminated by a plane wave at oblique incidence to be generated from the diffraction current for a reference cylinder of radius a_1 when excited at normal incidence. The reference data is generated using the exact solution for a cylinder with a moderate value of k_0a. In this Section, the validity and accuracy of the macromodel is examined by comparing the surface currents and near fields generated by the eigensolution with those of the macromodel for cylinders of radii larger than 1λ. Figure 5 shows the macromodelled diffraction current magnitude for cylinders of radii 10λ and 100λ excited at normal incidence compared with the exact solution for the TM case (*a*) and the TE case (*b*). The horizontal axes in both Figures are the normalised angular dimension or $\phi/2\pi$ with $\phi/2\pi = 0$, 0.5 corresponding to the top and bottom shadow boundaries respectively. The reference cylinder radius a_1 was chosen to be 20λ for the TM case and 50λ for the TE case.

The choice of radius for the reference cylinder is somewhat subjective but is based on maintaining high accuracy not only for cylinders of large electrical size, but also for cylinders down to a wavelength in radius. Both the gentle phase component and magnitude of the exact diffraction current have ripple in the deep-shadow region, caused by creeping wave effects, which can be seen in Fig. 5. The larger the cylinder, the smaller (in amplitude) and more localised these oscillations are to the deep-shadow region ($\phi/2\pi = -0.25$ in Fig. 5). For large cylinders, the level of diffraction current at which this ripple takes place is very low and it is therefore unlikely that this ripple would affect the near field anywhere except perhaps very near the surface in the deep shadow, and this implies that a larger cylinder, for the reference cylinder, is optimum for minimising the error between the exact solution and the macromodelled current. Smaller cylinders however, mainly resulting from more dominate creeping wave effects, have more variation in the diffraction current in the vicinity of the shadow boundary, as a function of k_0a, so too large a reference cylinder will not properly model the diffraction currents for cylinders of a smaller size. Thus the size of the reference cylinder is chosen to optimise accuracy as cylinder radius increases, while still being able to model cylinders of a more moderate radius.

Note that, in the reference data, the ripple in the deep-shadow region is removed from both the magnitude and gentle phase components of the diffraction current, and the remaining curve extended by assuming a continuation of the slope of the remaining data. In addition, the macromodelled diffraction current for the TE case (Fig. 5*b*) shows noticeable error for the 10λ cylinder in the lit region as normal incidence is approached ($\phi/2\pi = 0.25$) and is attributed to increasing error in the value of the weighting factor α for decreasing k_0a. In this region, the PO current is dominant and the error in the total current is still within the values described previously. In practice this has no effect on the accuracy of the total fields.

The error between the exact solution and the macromodel was investigated from a cylinder of 1λ radius up to a cylinder with radius of 200λ. In this range, the maximum error in magnitude in the total current (PO + diffraction) was -60 dB where the magnitude error is as previously defined or $e_m = 20\log||J_{ex}| - |J_{mm}||$. The phase error over this range was found to be less than 0.1° near the shadow boundary. Figure 7 shows an example of the macromo-

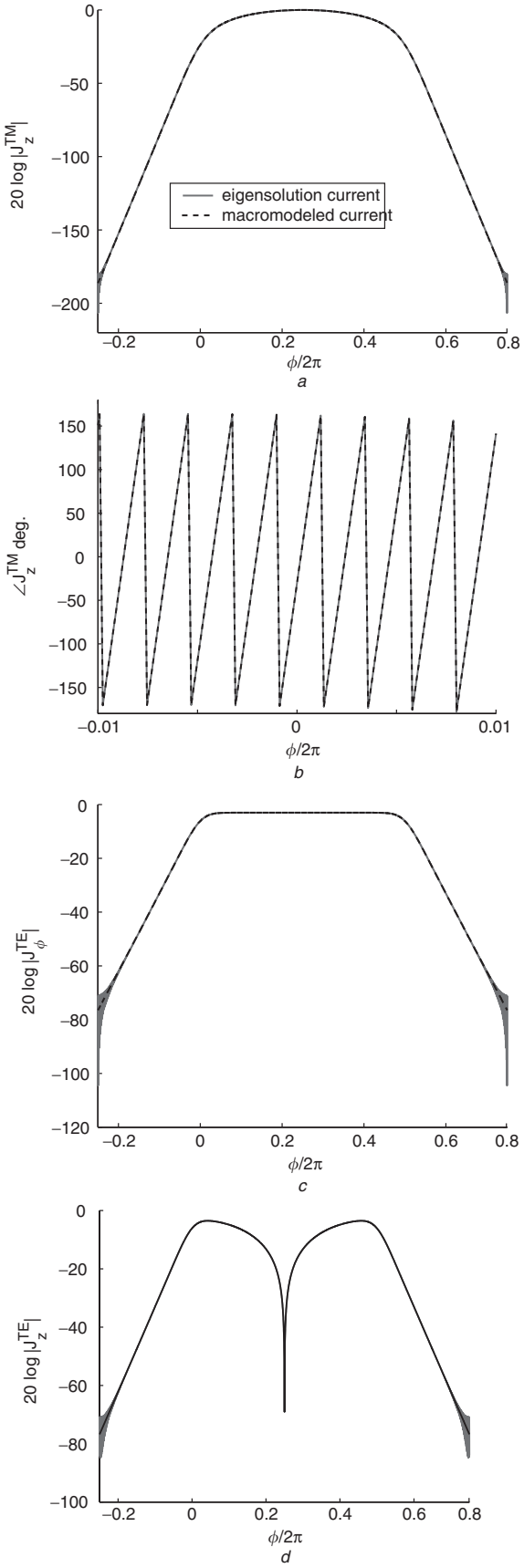

Fig. 7 *Total current, magnitude (dB) and phase (degrees) around full circumference of a 100λ PEC cylinder excited at oblique incidence angle, $\theta_i = \pi/4$, $(\phi/2\pi) = 0$ is equivalent to point on top of cylinder at the shadow boundary, with $(\phi/2\pi) = -0.25$ in the deep-shadow region*

a Magnitude of TM *z*-directed current
b Phase of TM z-directed current
c Magnitude of TE ϕ-directed current
d Magnitude of TE ϕ-directed current *z*-directed current

delled total current for a 100λ PEC cylinder excited at oblique incidence $\theta_i = \pi/4$ as compared with the exact current. Figure 7*a* and 7*b* show the magnitude and phase, respectively, of the total current for the TM case. Figure 7*c* shows the TE ϕ-directed current with Fig. 7*d* showing the additional z-directed current for the TE case at oblique incidence angle. As can be seen, the macromodel agrees very well with the exact solution in all cases.

The accuracy of the total fields (incident + scattered) generated by the macromodelled currents is shown in Fig. 8 for the TM case (*a*) and TE case (*b*). The data shown is for a 100λ cylinder excited at oblique incidence $\theta_i = \pi/4$, with fields 1λ off the cylinder surface plotted. Results from the macromodel are again compared with the exact solution. The scattered fields for both solutions are generated by applying the radiation integrals to the exact and macromodelled total currents. The fields generated by the macromodel are in good agreement over the entire range shown for both the TM and TE cases. The macromodel was shown to produce near fields that are highly accurate over a dynamic range of greater than 85 dB for cylinders of up to 200λ radius. The one exception to this is the TE ϕ-directed near fields at oblique incidence. As the incidence angle approaches grazing, the TE PO current is attenuated by a sin θ_i factor. As this happens, the accuracy of the TE ϕ-directed near fields is degraded. However, in the near field, the TE ρ-directed field is the dominate field component.

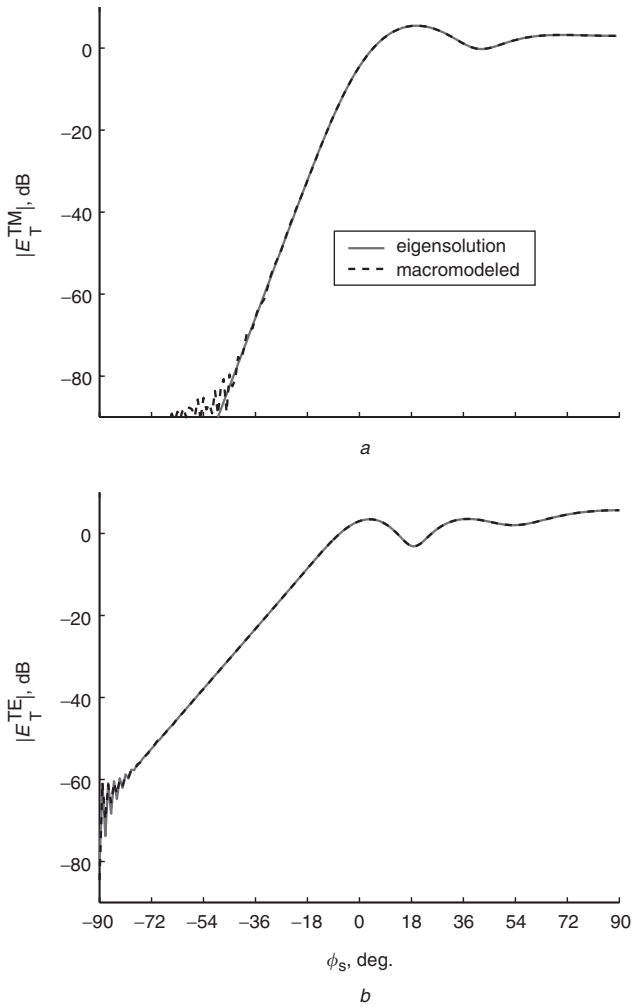

Fig. 8 *Magnitude (dB) of total E-fields 1λ off surface of a 100λ PEC cylinder excited by a plane wave at oblique incidence angle, $\theta_i = \pi/4$ with $-90°$ corresponding to deep shadow and $90°$ corresponding to normal incidence (deep lit)*

The results shown so far are for plane-wave incidence and near-field observation. By application of reciprocity [10], source and observation may be switched and the case of far fields generated from a point source (small dipole) radiating in the presence of a convex surface may be investigated. It can be shown through reciprocity that for identical point sources the following relationship holds:

$$\hat{l}_1 \cdot \boldsymbol{E}_2 = \hat{l}_2 \cdot \boldsymbol{E}_1 \tag{36}$$

where $\boldsymbol{E}_1$, $\boldsymbol{E}_2$ are electric fields caused by point sources with orientation $\hat{l}_1$, $\hat{l}_2$, respectively. If $\hat{l}_1$ is radiating in the far field of the convex surface and the corresponding electric field $\boldsymbol{E}_1$ is observed in the near field of the surface, it is equivalent to the plane-wave excitation problem with the incident plane wave weighted by the dipole field coefficients given by

$$\boldsymbol{E}_d^i(\boldsymbol{r}) = \frac{jl_1 k_0 Z_0 I_0}{4\pi r} e^{-jk_0 r}[\bar{\bar{I}} - k_1^i \cdot \hat{l}_1 \hat{k}_1^i] \tag{37}$$

where the vector $\boldsymbol{r} = r\hat{\boldsymbol{r}}$ is defined from the axis origin (always at the origin of the local radius of curvature) to the dipole position, l_1 is the dipole length, and I_0 is the dipole current magnitude. If l_2 is the orientation of a dipole radiating in the near field of the convex surface and knowing the plane-wave solution (36) can be solved for fields $\boldsymbol{E}_2$ which are the far fields generated by an infinitesimal dipole radiating in the presence of a convex surface. Applying this technique far-field results for the 2-D case were generated for an infinitesimal dipole radiating in the presence of a 20λ circular PEC cylinder, which can represent, the fuselage of an aircraft (12 m diameter at 1 GHz). The dipole is positioned at the top of the fuselage (x-axis, co-ordinates in Fig. 4 apply), 0.1λ away from the surface. Figure 9 shows the far-field patterns for three dipole orientations along with their corresponding positions. Figure 9*a* shows the result from a x-directed point source with Figs. 9*b* and 9*c* showing the results from a y- and z-directed dipole. Note that the observation point is at the minimum for the standard far-field criteria of $2D^2/\lambda$ where D is the diameter of the cylinder. Again, the fields generated from the macromodel are in excellent agreement with those generated by the exact solution.

5 Summary

Motivated by the shortcomings in existing high-frequency techniques, an alternative method was sought to calculate the diffraction currents induced on the surface of electrically large PEC cylinders when excited by a plane wave at oblique angles. An approach to determining these diffraction currents has been presented which is based on the asymptotic behaviour of the Fock currents. The method presented is highly accurate, producing total near fields with a dynamic range of over 85 dB. The macromodel developed is algebraic in nature and simple to implement. The block diagrams in Figs. 10 and 11 outline the procedure to generate both the reference data and macromodelled surface currents, respectively. To generate these macromodelled surface currents, the following steps are taken:

(i) Generate reference data at normal incidence ($a = 20\lambda$ for TM, $a = 50\lambda$ for TE) using the exact solution. Remove oscillations in reference data in deep shadow and approximate by extending slope of remaining data.

(ii) Apply (14)–(17) and (18)–(25) to the magnitude of the reference data for normal incidence to generate the magnitude of the diffraction current in the shadow and lit regions, respectively, for a cylinder of the desired radius.

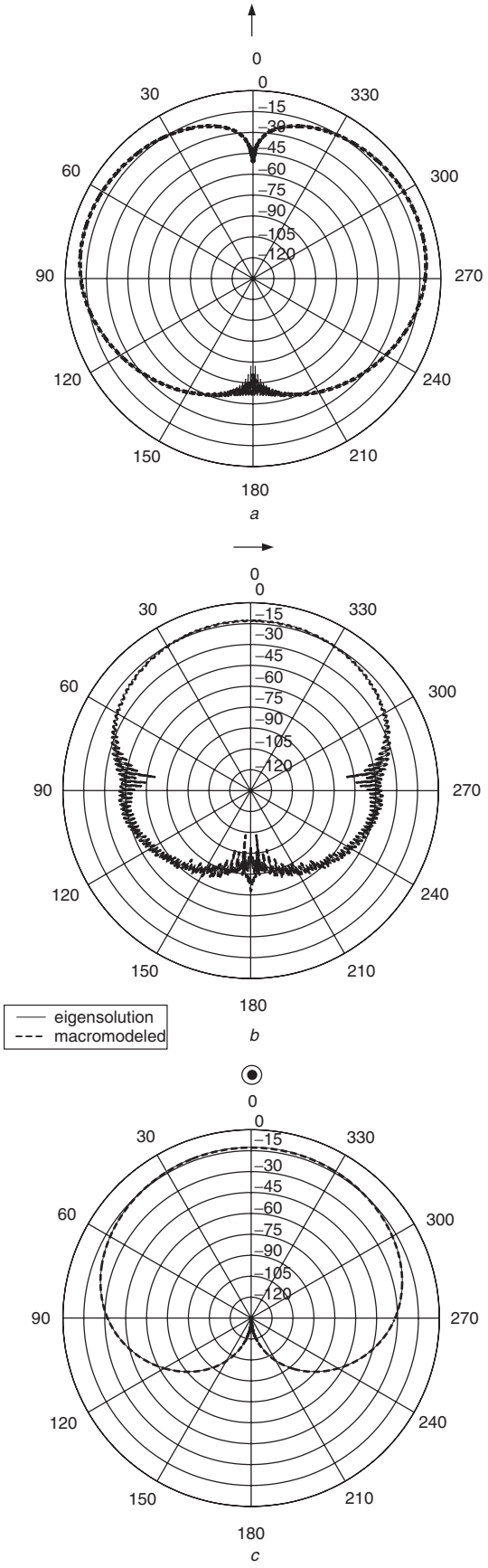

Fig. 9 *Magnitude (dB) of total far fields generated by a point source (small dipole) radiating in presence of 20λ PEC cylinder positioned 0.1λ off cylinder surface along the x axis (0° in plot) at $z = 0$*

Observation is at $2D^2/\lambda$ from cylinder centre and in x–y plane at $z = 0$

a $|E_\phi^S|$, far-field, x-directed dipole

b $|E_\phi^S|$, far-field, y-directed dipole

c $|E_z^S|$, far-field, z-directed dipole

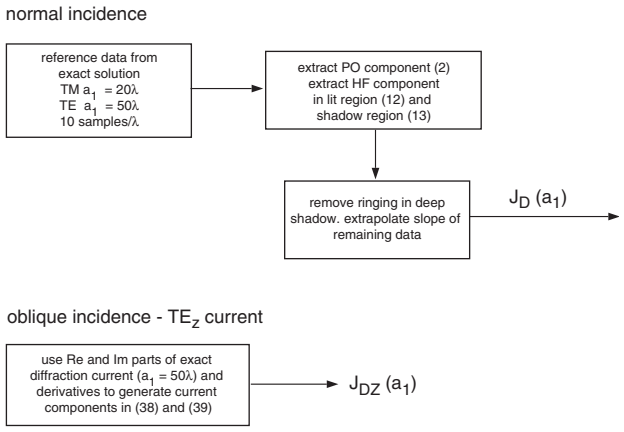

Fig. 10 *Generation of reference data: generate once, reference diffraction current $J_D(a_1)$*

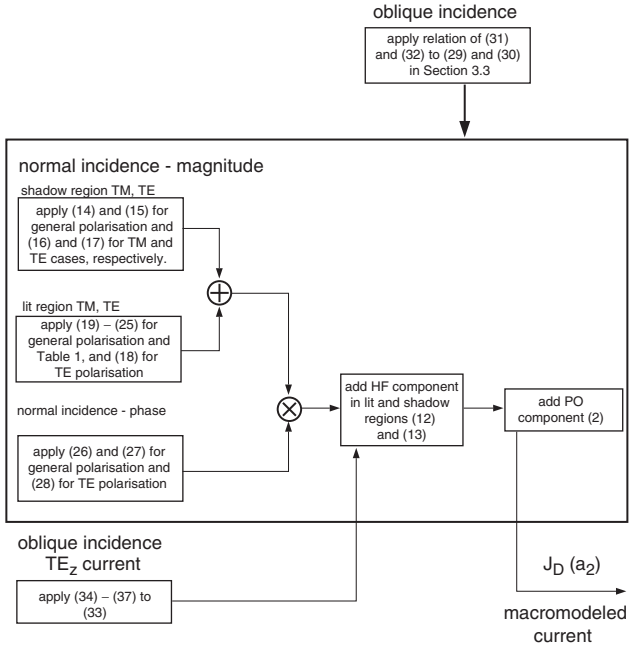

Fig. 11 *Procedure to implement macromodel: apply macromodel to reference current $J_D(a_1)$*

(iii) Apply (26)–(28) to the gentle phase component of the reference data for normal incidence to generate the gentle phase component in the shadow and lit regions, respectively.

(iv) To generate the TM z and TE ϕ currents for oblique incidence simply apply the modifications given in Section 3.3. For the additional z-directed current generated at oblique incidence for the TE case, apply (29)–(35) to the reference data for normal incidence to generate the derivative of the ϕ-directed current needed.

(v) Reference cylinder data is compressed as a function of ϕ when macromodelling surface diffraction current on cylinders of larger radius than that of the reference cylinder. Because of this, the macromodelled data does not extend over the full range of the cylinder (deep shadow to deep lit). To extend the macromodelled data to the full extent of the cylinder, simply assume a continuation of the slope in the lit and shadow regions, respectively.

(vi) If higher sampling of diffraction currents is required, apply simple linear interpolation to the magnitude and

gentle phase component of the macromodelled current to generate additional data points.

6 Acknowledgement

The authors gratefully acknowledge the support of the US Army Research Office under contract DAAH04-96-1-0377.

7 References

1 Balanis, C.A.: 'Advanced engineering electromagnetic' (Wiley & Sons, New York, 1989)
2 Bowman, J.J., Senior, T.B.A., and Uslenghi, P.L.E.: 'Electromagnetic and acoustic scattering by simple shapes' (Hemisphere, New York, 1969)
3 Keller, J.B.: 'Diffraction by a convex cylinder', *IRE Trans. Antennas Propag.*, 1956, **4**, (3), pp. 312–321
4 Pathak, P.H.: 'An asymptotic analysis of the scattering of plane waves by a smooth convex cylinder', *Radio Sci.*, 1979, **14**, (3), pp. 419–435
5 Hussar, P., and Albus, R.: 'On the asymptotic frequency behavior of uniform GTD in the shadow region of a smooth convex surface', *IEEE Trans. Antennas Propag.*, 1991, **39**, (12), pp. 1672–1680
6 Fock, V.A.: 'The field of a plane wave near the surface of a conducting body', *J. Phys. USSR.*, 1946, **10**, (5), pp. 399–409
7 Pearson, L.W.: 'A scheme for automatic computation of Fock-type integrals', *IEEE Trans. Antennas Propag.*, 1987, **35**, (10), pp. 1111–1118
8 Logan, N.A.: 'General research in diffraction theory vols. 1 & 2'. Technical Reports LMSD-288088 & 288089; Lockheed Missiles and Space Division, Sunnyvale, CA, 1959
9 Ufimtsev, P.Y.: 'Method of edge waves in the physical theory of diffraction'. Technical Report (English translation available) from NATS, Springfield, VA 22161; AD733203, Sovyetskoye Radio, Moscow, Russia, 1962
10 Harrington., R.F.: 'Time-harmonic electromagnetic fields' (McGraw-Hill, New York, 1961)